Journal of Molecular Structure 1352 (2026) 144488

Contents lists available at ScienceDirect

Journal of Molecular Structure

journal homepage: www.elsevier.com/locate/molstr

Deciphering supramolecular synthons in OXYMA-B salts: Crystallographic characterization and theoretical evaluation of hydrogen bond networks

Mahdi Jemai [a,b], Rafael Barbas [c], Miquel Barceló-Oliver [d], Houda Marouani [b], Fernando Albericio [e], Antonio Frontera [d,*], Rafel Prohens [a,*]

[a] Laboratory of Organic Chemistry, Faculty of Pharmacy and Food Sciences, University of Barcelona, Avda. Joan XXIII, 08028 Barcelona, Spain
[b] Laboratory of Material Chemistry, LR13ES08, Faculty of Sciences of Bizerte, University of Carthage, 7021 Bizerte, Tunisia
[c] Unitat de Polimorfisme i Calorimetria, Centres Científics i Tecnològics, Universitat de Barcelona, Baldiri Reixac 10, 08028 Barcelona, Spain
[d] Department of Chemistry, University of Balearic Islands, 07122 Palma, Spain
[e] CIBER-BBN, Networking Centre on Bioengineering, Biomaterials and Nanomedicine, and Department of Organic Chemistry, University of Barcelona, Martí i Franqués 1-11, 08028 Barcelona, Spain

ARTICLE INFO

Keywords:
Crystal engineering
Oxyma-B
Molecular salts
Hydrogen bonding
Supramolecular synthons
DFT calculations

ABSTRACT

Four new crystal structures of OXYMA-B in its anionic form have been synthesized and structurally characterized via single-crystal X-ray diffraction. The new salts incorporate protonated amine-based cations including 1-phenylpiperazine (1PP), 1,4-dioxa-8-azaspiro[4.5]decane (DASD), ethylenediamine (ETDA), and pyrrolidine (Pyr), which function as efficient hydrogen bond (H-bond) donors. The electron-rich nature of the OXYMA-B anion provides multiple sites for H-bond acceptance, leading to diverse supramolecular synthons including $R_1^2(5)$, $R_1^2(6)$, $R_4^2(8)$ and $R_4^3(12)$. The theoretical component of this study is based on density functional theory (DFT) calculations to dissect and characterize the individual H-bonded synthons using the quantum theory of atoms in molecules (QTAIM) framework. Additionally, interaction energies of discrete H-bonds have been quantified to rationalize their strength and directional preferences, showing that directional NH···O bonds contribute the most to the stability of the assemblies, with ancillary contacts playing a secondary but supportive role. The total interaction energies range from –34.0 to –50.0 kcal/mol, underscoring the critical role of hydrogen bonding in dictating the supramolecular architectures. This combined experimental–computational approach sheds light on the structural determinants driving supramolecular organization in OXYMA-B-based salts and highlights their potential for crystal engineering applications.

1. Introduction

Crystal engineering is a dynamic field focused on the rational design and construction of molecular solids through the knowledge and exploitation of non-covalent interactions (NCIs), whose ability to harness classical and non-classical interactions makes them ideal candidates for investigating the principles of supramolecular assembly [1–3]. The most widely explored crystalline supramolecular systems are salts and cocrystals, which offer a powerful approach to tailor physicochemical properties such as solubility, stability, and reactivity without altering covalent frameworks [4–8]. Molecular salts are particularly interesting due to their ionic character which confers the capacity for strong hydrogen bonding, and the ability to generate diverse supramolecular motifs, making them highly valuable in pharmaceuticals, functional materials, and supramolecular chemistry [9,10]. Moreover, the formation of molecular salts enables the investigation of intermolecular interactions that arise specifically when proton donors and acceptors combine to generate charged species within the crystal lattice. This process directly influences the physical and chemical properties of the resulting materials, which differ significantly from those of their individual neutral constituents. The presence of ionic interactions provides an alternative framework in which classical and non-classical intermolecular forces may be either reinforced or attenuated, thereby offering deeper insight into the principles governing the packing of compounds in both neutral and charged states [11–13].

From a crystal engineering point of view, Oxyma-B offers a structurally singular framework, derived from the well-known peptide coupling additive Oxyma-Pure. Oxyma-B is a six-membered cyclic oxime

* Corresponding authors.
E-mail addresses: toni.frontera@uib.es (A. Frontera), rafel_prohens@ub.edu (R. Prohens).

https://doi.org/10.1016/j.molstruc.2025.144488
Received 8 September 2025; Received in revised form 20 October 2025; Accepted 20 October 2025
Available online 24 October 2025

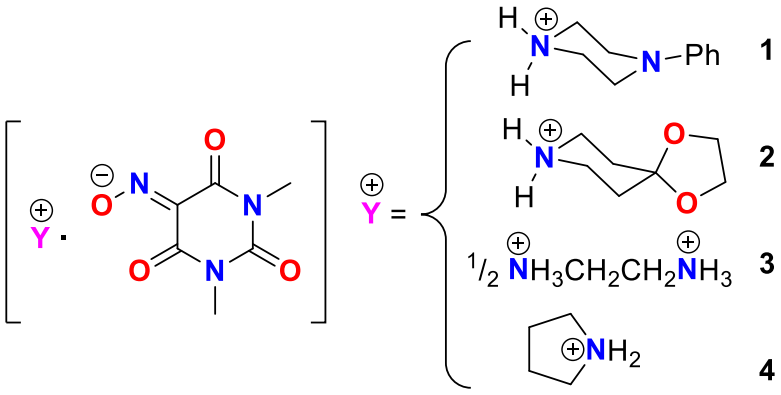

Scheme 1. Oxyma-B salts reported in this work and compound numbering scheme.

bearing electron withdrawing groups that significantly modulate its electronic landscape [14–17]. This unique configuration equips it with multiple potential interaction sites in the solid state [17]. However, the role of Oxyma-B as a crystalline molecular salt former, remains underexplored. This has motivated us to explore the use of both cyclic and acyclic amines (Scheme 1) to prepare single crystals of their salts with Oxyme B, anticipating that their restricted geometries and varied electronic environments might offer distinct opportunities to modulate the efficiency of supramolecular assembly and packing.

Owing to its diverse hydrogen bond accepting ability, the anionic form of Oxyma-B presents a versatile scaffold for the formation of stable supramolecular assemblies with a variety of amine-based protonated cations. While the crystal structures reveal rich and diverse hydrogen bonding patterns, a deeper understanding of the nature and energetics of these synthons requires detailed computational insight. In this context, we complement our crystallographic findings with a density functional theory (DFT) investigation focused on the characterization of the key hydrogen bonds using QTAIM analysis. This theoretical framework will allow us to quantify the individual interaction energies and gain insight into the dominant supramolecular forces that govern the assembly of these salts in the solid state.

2. Experimental section

2.1. Synthesis and crystallization

Each molecular salt was prepared by slow evaporation of equimolar solutions of Oxyma-B (50 mg) and the respective amine coformer. Each mixture was dissolved in 6 mL of an appropriate solvent or solvent mixture and stirred at room temperature for 30 minutes to ensure homogeneity. For 1-phenylpiperazine the mixture was dissolved in ethanol, with pyrrolidine in a 1:1 ethanol/acetone mixture, while with 1,4-Dioxa-8-azaspiro[4.5]decane and ethylenediamine in a 1:1:1 ethanol/acetone/THF. The resulting solutions were allowed to evaporate slowly at room temperature. A few days later, crystals suitable for SCXRD were obtained. High-quality single crystals were carefully selected under an optical microscope prior to X-ray analysis.

2.2. Crystal structure determination

Single-crystal X-ray diffraction data for the newly obtained molecular salts were collected using a Bruker D8 VENTURE diffractometer equipped with a microfocus Incoatec IμS DIAMOND source emitting Cu Kα radiation (λ = 1.54178 Å), along with Helios MX multilayer optics.

Table 1
Crystallographic data of salts 1-4.

Compound	1	**2**	**3**	**4**
Empirical formula	$C_6H_6N_3O_4{\cdot}C_{10}H_{15}N_2$	$C_6H_6N_3O_4{\cdot}C_7H_{14}NO_2$	$2(C_6H_6N_3O_4){\cdot}C_2H_{10}N_2$	$C_6H_6N_3O_4{\cdot}C_4H_{10}N$
Formula weight	347.38	328.33	430.39	256.27
Temperature (K)	100	100	299	100
Crystal system	Triclinic	Triclinic	Monoclinic	Monoclinic
Space group	*P-1*	*P-1*	$P2_1/c$	$P2_1/c$
a (Å)	6.5928 (6) Å	6.7672 (4)	15.2464 (3)	6.9555 (2)
b (Å)	10.3576 (9)	9.9846 (7)	6.8896 (2)	14.7181 (4)
c (Å)	12.8777 (11)	11.6985 (8)	9.0947 (2)	11.8108 (3)
α (°)	91.450 (3)	96.399 (2)	90	90
β (°)	99.904 (3)	97.687 (2)	98.919 (1)	90.437 (1)
γ (°)	107.732 (3)	106.425 (2)	90	90
V(Å^3)	822.27 (13)	742.05 (9)	943.77 (4)	1209.06 (6)
Z	2	2	2	4
θ (°)	3.5_68.4	5.6_68.2	2.9_68.3	6.4_68.3
Reflections collected	16192	47 569	11 475	17 288
Independent reflections	2939	2 546	1 724	2 210
R*int*	0.069	0.053	0.054	0.045
Reflections with I > 2σ(I)	2794	2 545	1 605	2 076
Refined parameters	236	238	150	174
Restraints	0	13	0	2
Δρ *min* (*e* Å^{-3})	-0.41	-0.21	-0.23	-0.22
Δρ *max* (*e* Å^{-3})	0.43	0.28	0.39	0.37
Density (calc. Mg/m3)	1.403	1.469	1.515	1.408
Final R indices [I>2σ(I)]	R1= 0.078	R1= 0.042	R1= 0.045	R1= 0.057
	WR2= 0.237	WR2= 0.115	WR2= 0.131	WR2= 0.151
CCDC	**2479360**	**2479361**	**2479359**	**2479358**

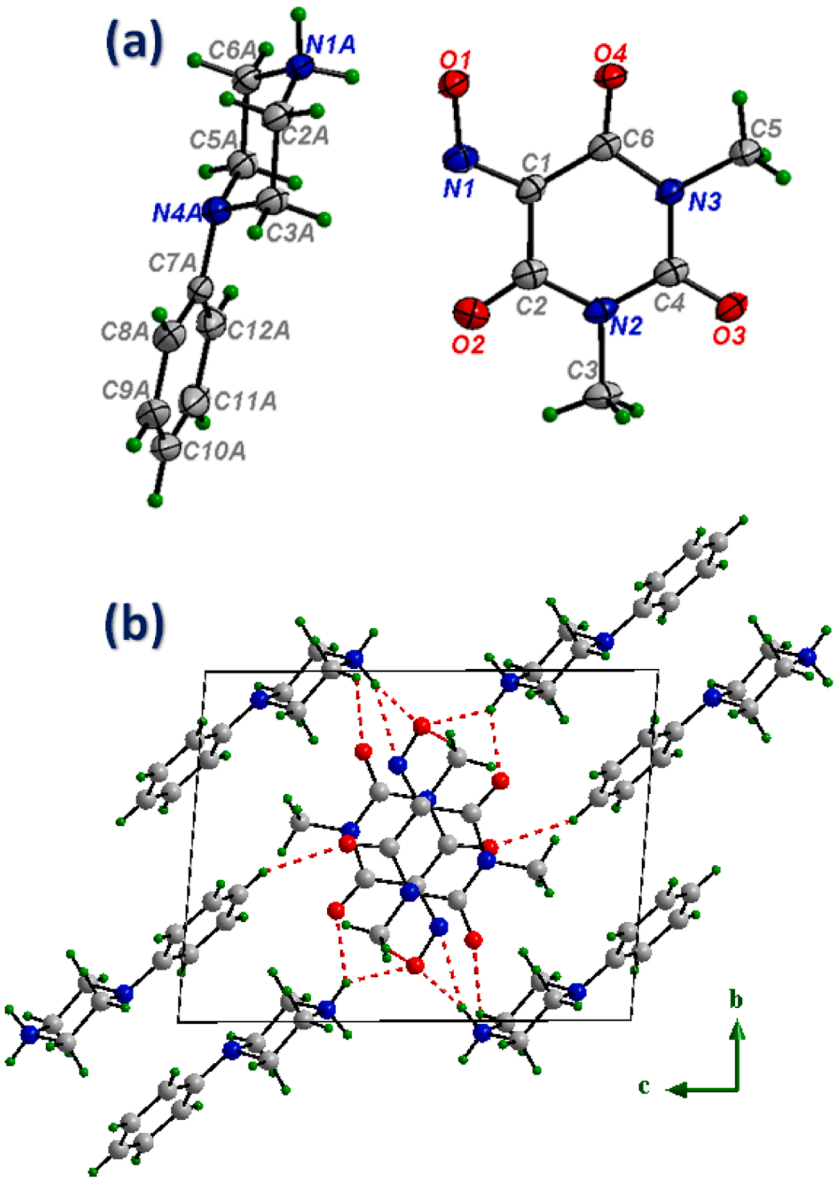

Fig. 1. (a) Asymmetric unit of 1-phenylpiperazine/Oxyma-B salt (1) with the labeling scheme. Thermal ellipsoids are drawn at the 35% probability level**; (b)** Crystal packing of salt (1) viewed along the a-axis, showing layered arrangement and hydrogen-bonding interactions between cations and anions.

Data reduction and cell refinement were carried out using the APEX5 software [18]. A multi-scan absorption correction was applied through the SADABS-2016/2 program [18].

Structure solution was performed via intrinsic phasing using SHELXT-2018/2, and all structures were refined against F^2 using full-matrix least-squares methods implemented in SHELXL-2019/3, all within the Olex2-1.5 [19,20]. Non-hydrogen atoms were refined anisotropically. Hydrogen atoms attached to nitrogen were located from difference Fourier maps and refined without constraints, whereas those bound to carbon atoms were introduced in idealized positions and treated using a riding model, with $U_{iso}(H) = 1.2U_{eq}(C)$. In compounds 2 and 3 some disorder was found: i) in compound 2, the 1,4-dioxolane ring of the DASD molecule has 2 disordered carbon atoms (52 and 48 % occupancy for each part); in compound 3 the whole ring from OXYMA-B molecule is rotated trough the N1-C1 bond (52 and 48 % occupancy for each part). Some restraints have been applied to those two compounds to correctly split the disordered molecules (SAME/SADI). All structures were examined for higher symmetry using PLATON [21]. Graph-Set analysis [22] was conducted using DIAMOND (version 3.2k) [23]. Crystallographic details for the salts are compiled in Table 1.

2.3. Theoretical methods

All quantum chemical calculations were carried out using the Gaussian 16 software package (Revision C.01) [24]. The crystallographic coordinates obtained from X-ray diffraction experiments were used without further geometry optimization in order to preserve the experimentally observed supramolecular arrangements. The electronic structure calculations were performed at the PBE0-D3/def2-TZVP level of theory [25–27], which has been shown to reliably describe non-covalent interactions including hydrogen bonding and dispersion effects.

Molecular electrostatic potential (MEP) surfaces were computed at the same level of theory to visualize the distribution of electron density and identify potential hydrogen-bond acceptor sites in the OXYMA-B anion. Topological analysis of the electron density was conducted within the framework of Bader's Quantum Theory of Atoms in Molecules (QTAIM) using the wavefunction files generated by Gaussian and

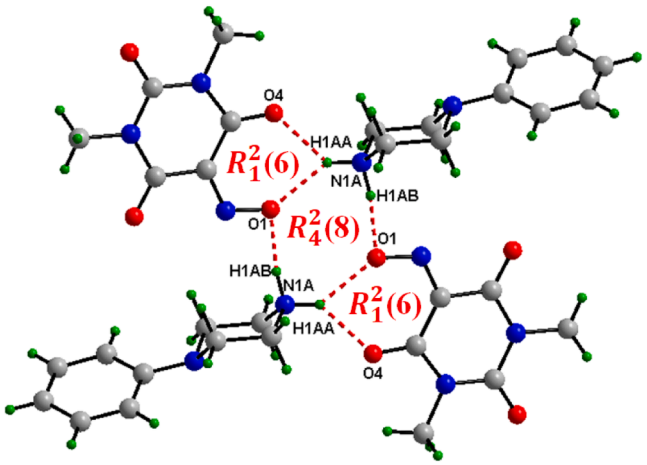

Fig. 2. Supramolecular synthons in the crystal structure of salt (1): $R_4^2(8)$ and $R_1^2(6)$ motif formed via NH···O hydrogen bonding.

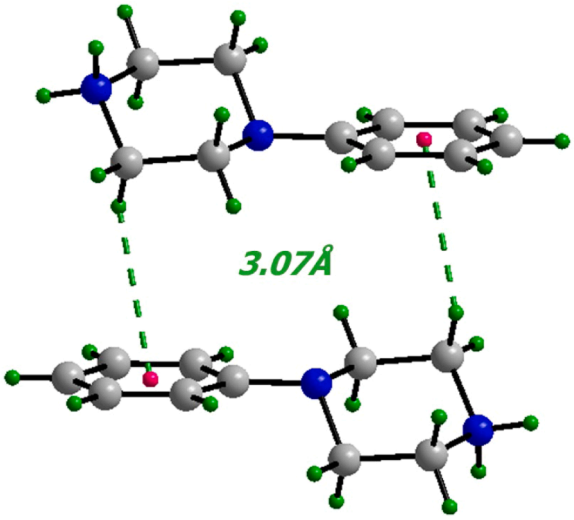

Fig. 3. CH···π interactions between adjacent 1-phenylpiperazine cations in salt (1), showing hydrogen-to-centroid distances.

analyzed with the AIMAll software (version 19.10.12) [28,29]. Bond critical points (BCPs), bond paths, and potential energy density (V) values at the BCPs were extracted for all relevant hydrogen-bond interactions.

The interaction energies of individual hydrogen bonds were estimated using the empirical relationship proposed by Espinosa et al. [30], which correlates the potential energy density at the BCP with the interaction energy via the equation $E \approx 0.5 \times V$. This method provides a reliable estimate of the strength of hydrogen bonds directly from the QTAIM descriptors.

3. Results and discussion

As expected, the four crystal forms confirmed the formation of salts through proton transfer from the acidic hydroxyl group of Oxyma-B to the basic nitrogen site of the amine. This deprotonation leads to an anionic Oxyma-B moiety and a protonated amine, forming robust ionic frameworks stabilized by a rich array of supramolecular interactions, which are the subject of study of this work.

3.1. Structural description and supramolecular details

3.1.1. 1-phenylpiperazine / Oxyma-B salt (1)

The molecular salt formed between 1-phenylpiperazine and Oxyma-B (1), depicted in Fig. 1(a), crystallizes in the triclinic crystal system with space group *P-1*. The asymmetric unit comprises one molecule of each constituent, yielding a formula unit count of Z = 2. Fig. 1(b) presents the crystal packing of salt (1) viewed according to $\vec{a}$ direction. The structure reveals an organized arrangement in which the organic cations are aligned at z = 1, while the anionic Oxyma-B moieties are intercalated around z = 1/2, forming layers parallel to the (*bc*) plane. These anions bridge adjacent cationic chains through a network of NH···O, NH···N and CH···O hydrogen bonds, resulting in a supramolecular framework stabilized by directional intermolecular interactions.

As illustrated in Fig. 2, the interaction between 1-phenylpiperazine and Oxyma-B via NH···O hydrogen bonding generates a primary supramolecular synthons of $R_4^2(8)$ and $R_1^2(6)$ type.

As depicted in Fig. 3, weak intermolecular interactions are also observed between the 1-phenylpiperazine cations separately. Thus, the stabilization and spatial arrangement of the cations are additionally reinforced by CH···π interactions. These contacts are established between the electron rich phenyl ring of one cation and one of the hydrogens adjacent to the charged nitrogen atom, with hydrogen-to-centroid distances of 3.073(4) Å and a CH···centroid angle of 123.10 (1) °.

The Oxyma-B anions in salt (1) (Fig. 4) adopt an orderly packing arrangement stabilized by a combination of non-covalent interactions. In addition to weak CH···O hydrogen bonds, the anions engage in aromatic interactions. Notably, parallel face-to-face stacking is observed

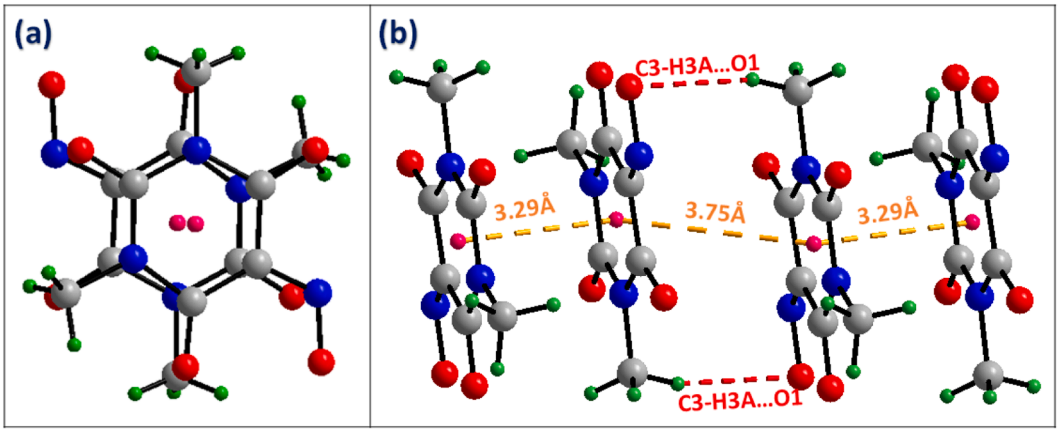

Fig. 4. Packing features of Oxyma-B anions in compound 1: (a) Face-to-face stacking, (b) detailed view of the non-covalent interactions stabilizing the anionic moieties.

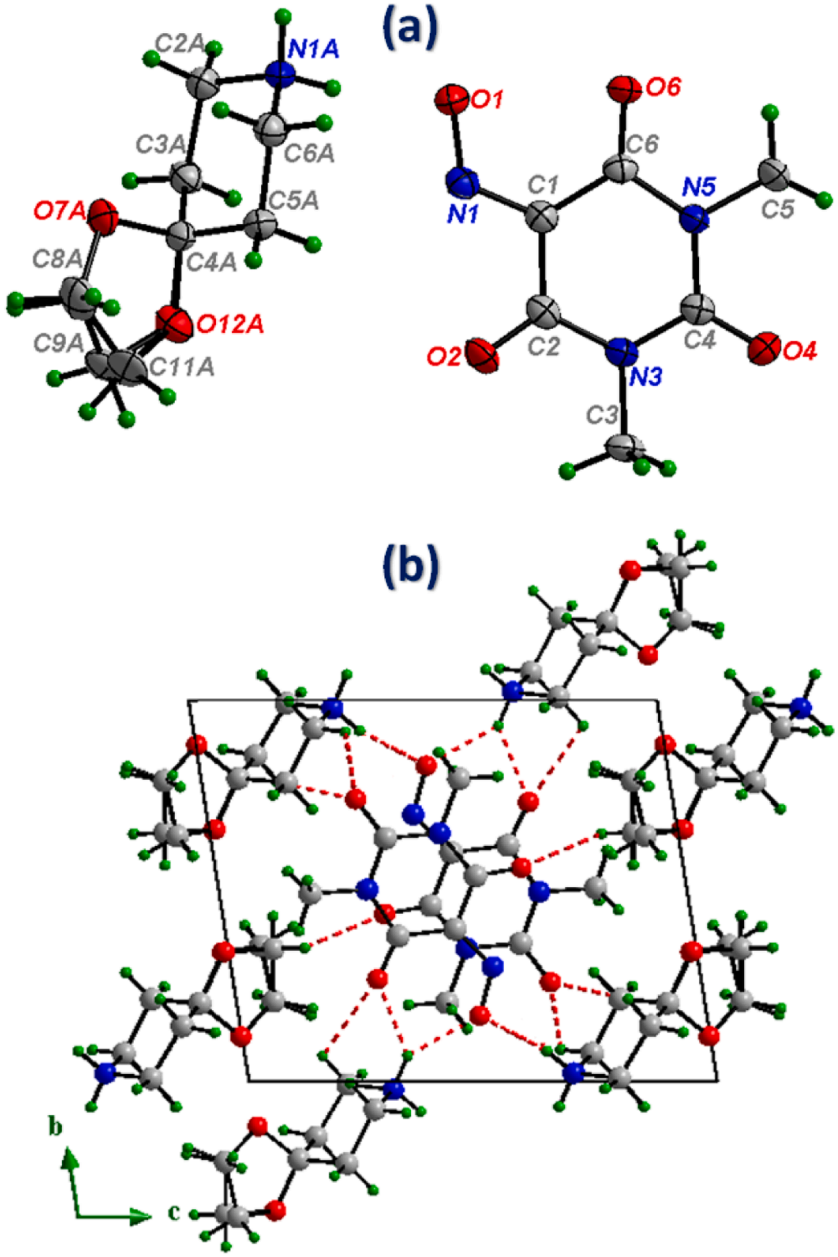

Fig. 5. **(a)** Molecular structure of salt (2) showing atomic labels and 1,4-dioxolane ring disorder over C9A/C11A sites. Ellipsoids are drawn at the 35% probability level; **(b)** Crystal packing of salt (2) viewed along the a-axis.

between adjacent aromatic rings (Fig. 4a), with centroid-to-centroid separations of 3.290(3) and 3.754(4) Å. These distances fall within the range (3.3–3.8 Å) reported for effective π···π interactions in purely organic systems [31].

3.1.2. 1,4-Dioxa-8-azaspiro[4.5]decane/ Oxyma-B salt (2)

The molecular salt formed between 1,4-dioxa-8-azaspiro[4.5]decane (DASD) and Oxyma-B, referred to as salt (2), crystallizes in the triclinic crystal system with space group *P-1*. The asymmetric unit comprises one molecule of DASD and Oxyma-B (Z = 2). As depicted in Fig. 5(a), one carbon atom within the 1,4-dioxolane ring of the DASD molecule is positionally disordered and was modeled over two sites, C9A and C11A, with refined occupancy factors of 0.535 and 0.465 respectively. The hydrogen atoms attached to the nearby C8A carbon are also disordered with the same occupancies. The crystal packing of salt (2), shown in Fig. 5 (b), reveals that the DASD cations are aligned in layers at z = 0, while the Oxyma-B anions are intercalated at z = 1/2, acting as bridges between adjacent DASD layers through multiple hydrogen bonding interactions, including NH···O and CH···O.

The extensive hydrogen bonding framework gives rise to several supramolecular synthons, as illustrated in Fig. 6a, ring motifs $R_4^4(22)$ emerge from cation-anion contacts; Fig. 6b displays the motif $R_4^4(24)$ and Fig. 6c highlights additional hydrogen-bonded synthons of types $R_4^2(8)$ and $R_1^2(6)$.

The anion···anion assembly in salt (2) is stabilized by two types of non-covalent interactions (Fig. 7). CH···O H-bonding between neighboring Oxyma-B anions are complemented by face-to-face stacking between adjacent Oxyma-B rings, with a centroid-to-centroid separation of 3.450(3) Å.

3.1.3. Ethylenediamine / Oxyma-B salt (3)

The crystal structure of the Ethylenediamine/Oxyma-B salt (3), illustrated in Fig. 8(a), crystallizes in the monoclinic system the $P2_1/c$

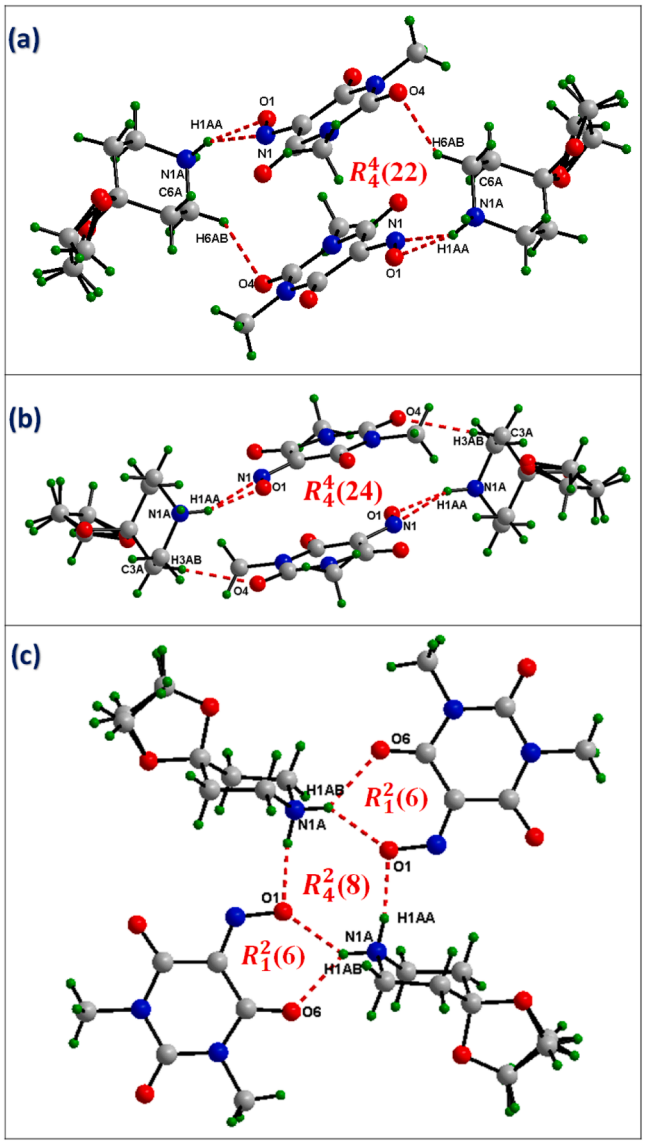

Fig.. 6. Hydrogen-bonding synthons in the crystal packing of salt (2): (a) $R_4^4(22)$; (b) $R_4^4(24)$; (c) $R_4^2(8)$ and $R_1^2(6)$.

space group. The asymmetric unit consists of one Oxyma-B and half of ethylenediamine molecule (Z = 2), where the diamine is a centrosymmetric molecule with an inversion center located at the midpoint of the

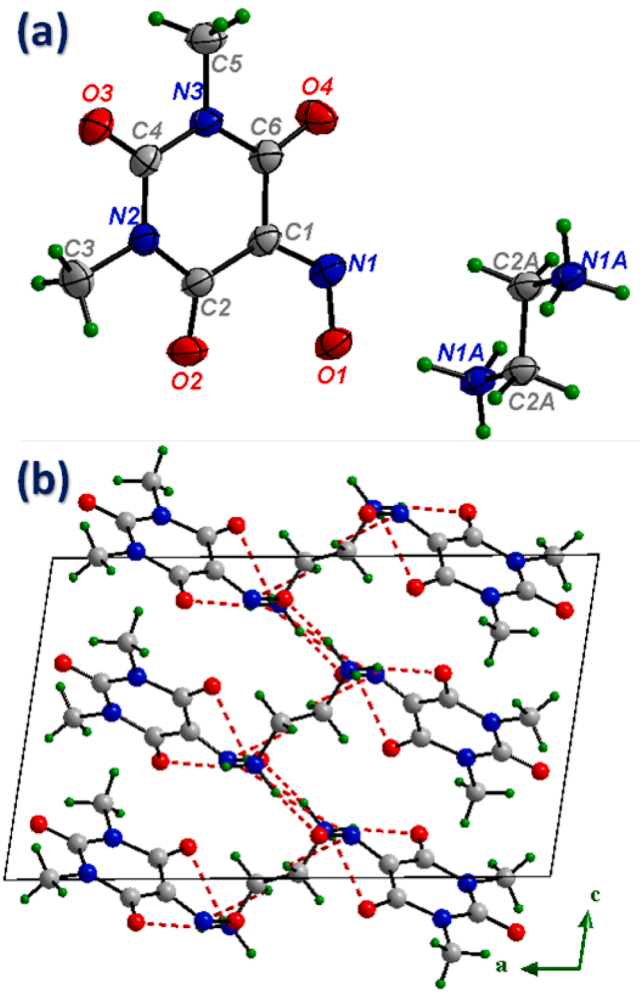

Fig. 8. (a) ORTEP representation of the asymmetric unit of the Ethylenediamine/Oxyma-B salt (3). Ellipsoids correspond to a 35% probability level; **(b)** Crystal packing of salt (3) viewed along the (*ac*) plane, showing the HB network interlinking ETDA cations and Oxyma-B anions.

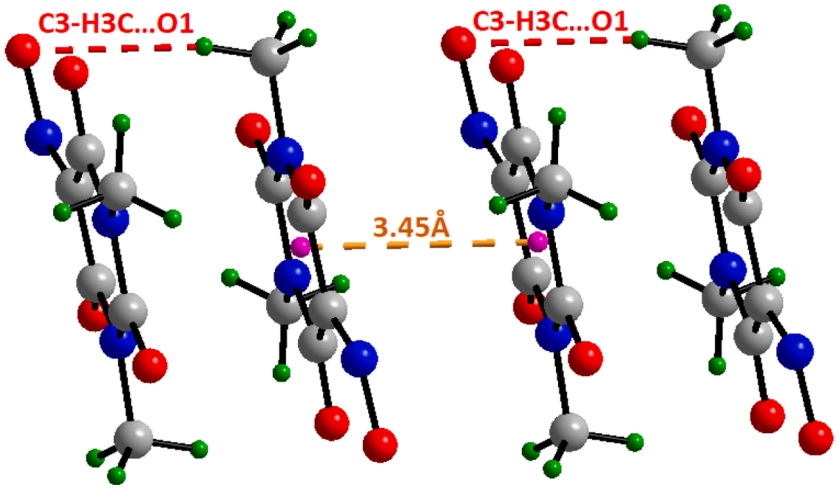

Fig. 7. Anion···anion intermolecular interactions in salt (2).

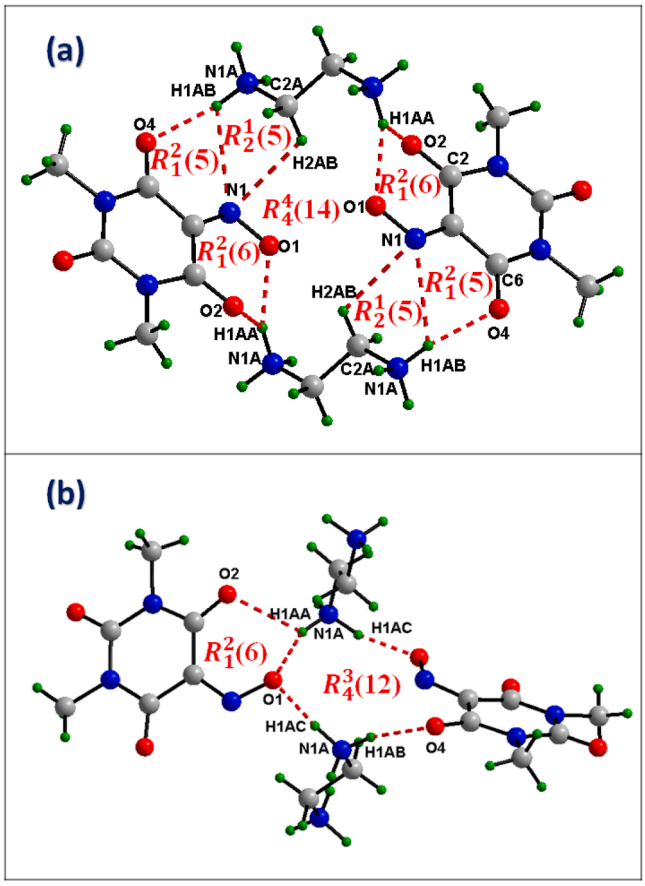

Fig. 9. Supramolecular synthons formed in the crystal structure of salt (3).

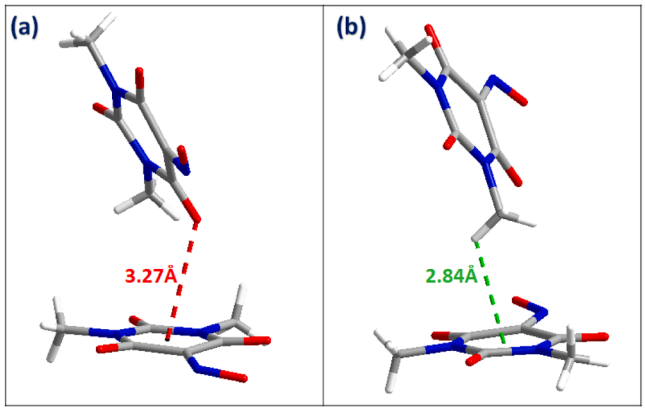

Fig. 10. Anion···anion aromatic interactions: **(a)** O···π and **(b)** CH···π.

C2A–C2A bond. Fig. 8(b) presents the crystal packing of salt (3) viewed along the (*ac*) plane. The structure is stabilized by an extensive hydrogen-bonding network involving NH···O, NH···N, and CH···N interactions where Oxyma-B anions are positioned at x = 1/4 and x = 3/4, forming layers interconnected by ethylenediammonium (ETDA) dications, which act as bridges between adjacent anionic layers.

The dense hydrogen bonding network leads to the formation of multiple distinct supramolecular synthons. As illustrated in Fig. 9a, smaller ring motifs such as $R_1^2(5)$, $R_2^1(5)$ and $R_1^2(6)$ surround a larger, central $R_4^4(14)$ motif. Fig. 9b highlights the additional motifs $R_4^3(12)$, all of which result from anion···cation interactions within the crystal structure.

Again aromatic interactions contribute significantly to the

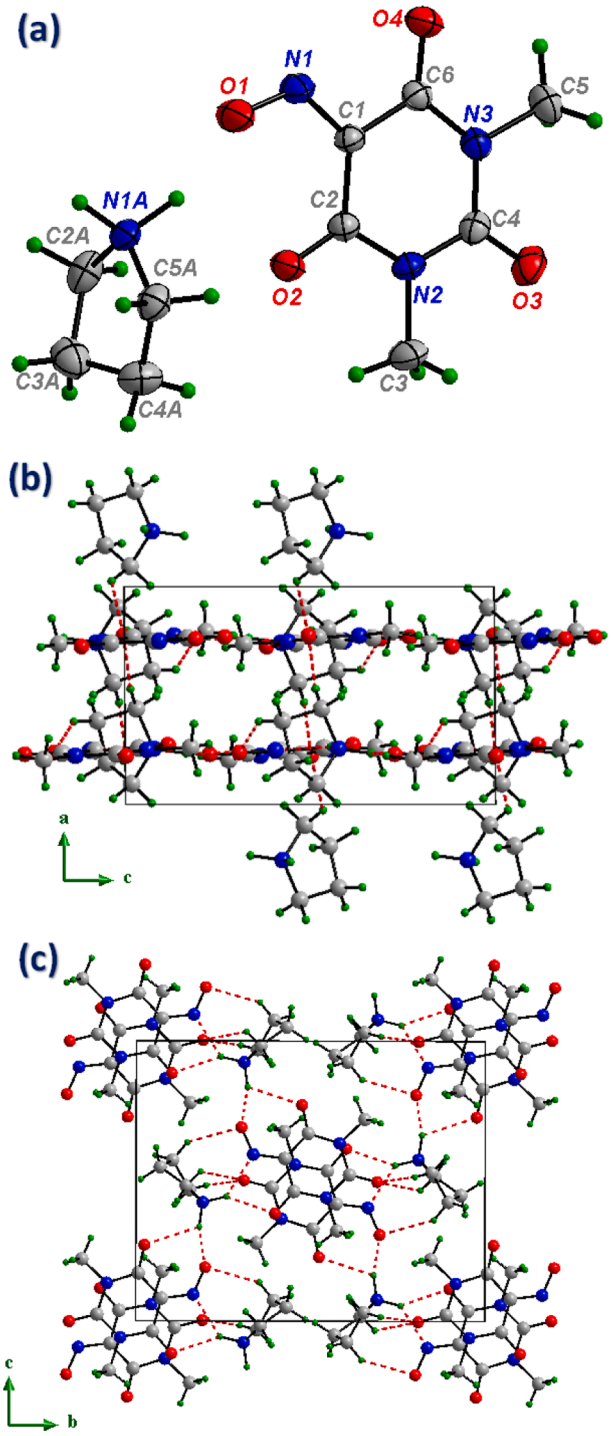

Fig. 11. (a) Asymmetric unit of Pyrrolidine/Oxyma-B salt (4) showing the molecular components and atom labeling (Thermal ellipsoids are drawn at the 35% probability level); Crystal packing of salt (4): **(b)** view along the (*ac*) plane showing orthogonal anion-cation layers; **(c)** view along the (*bc*) plane with pyrrolidine intercalated via NH···O, NH···N, and CH···O hydrogen bonds.

anion···anion assembly in salt (3), as illustrated in Fig. 10, in which Oxyma-B anions forms lone pair (O)···π contacts, with oxygen-to-centroid distance equal to 3.270(1) Å. Additionally, CH···π contacts are present, with a hydrogen-to-centroid distance of 2.842(0) Å and a CH···centroid angle of 120.10(0) °, further reinforcing the supramolecular connectivity.

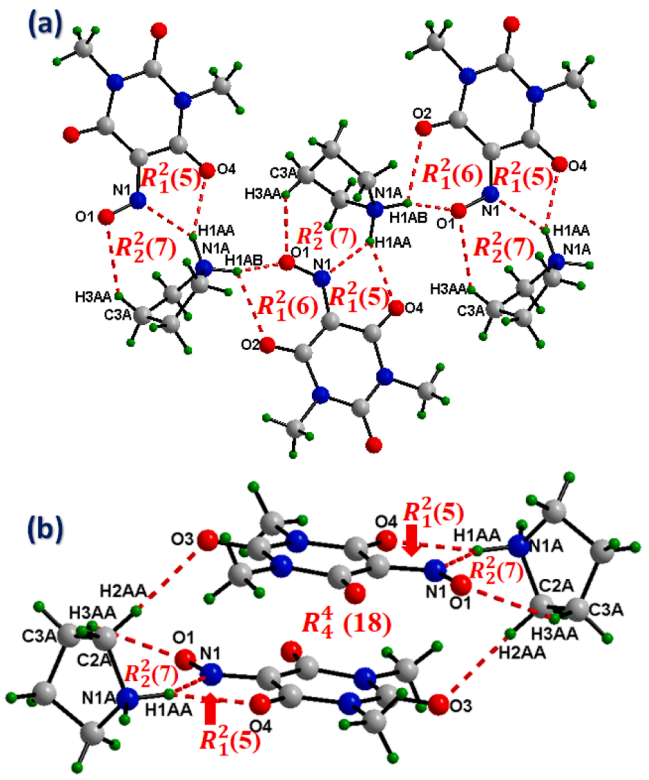

Fig. 12. Supramolecular synthons in salt (**4**): (a) Hydrogen-bonding motifs $R_1^2(5)$, $R_1^2(6)$ and $R_2^2(7)$;(b) extended supramolecular motif $R_4^4(18)$ involving paired Oxyma-B and pyrrolidine units.

3.1.4. *Pyrrolidine / Oxyma-B salt (4)*

Pyrrolidine/Oxyma-B salt (4), illustrated in Fig. 11(a), crystallizes in the monoclinic system, space group $P2_1/c$, with the asymmetric unit comprising one independent molecule each of Oxyma-B and Pyrrolidine (Z = 4). The crystal packing of salt (4), projected along the (*ac*) plane (Fig. 11b), reveals an alternating layered structure, where the cationic and anionic components form distinct planes oriented nearly perpendicular to one another. Specifically, Oxyma-B anions are arranged parallel to the (*bc*) plane and located at x = 1/4 and x = 3/4, whereas pyrrolidine cations occupy layers at x = 0 and x = 1/2. A more detailed projection along the (*bc*) plane (Fig. 11c) clearly illustrates that pyrrolidine molecules are intercalated between Oxyma-B anions, contributing to the crystal stability through a network of NH···O, NH···N, and CH···O hydrogen bonds.

The hydrogen bonding network in salt (4) is defined by a combination of contacts leading to different types of supramolecular synthons. As shown in Fig. 12a, these interactions organize the components into several motifs, which include $R_1^2(5)$, $R_1^2(6)$ and $R_2^2(7)$. In addition, Fig. 12b highlights a larger supramolecular motif $R_4^4(18)$ generated by an association of pairs of Oxyma-B anions and pyrrolidine cations.

3.2. *Hirshfeld surface analysis*

To gain deeper insight into the nature and contributions of intermolecular interactions governing the solid-state architecture of the Oxyma-B salts, Hirshfeld surface (HS) analysis was conducted using *CrystalExplorer* software [32,33]. This approach enables both qualitative and quantitative visualization of close contacts and interaction patterns within the crystal lattice. The resulting two-dimensional fingerprint plots provide a comparative overview of the key intermolecular interactions present across the series.

Fig. 13 presents the Hirshfeld surface (HS) analysis of Oxyma-B molecules in salts formed with amines (compounds 1-4). The analysis was conducted by selecting only the Oxyma-B molecule to specifically assess its supramolecular susceptibility and interaction behavior.

On the left side of the figure, the 3D d_{norm} surfaces highlight prominent hydrogen bonding regions as red spots, corresponding to close contacts involving O···H/H···O and N···H/H···O interactions. These features are clearly represented in the associated 2D fingerprint plots on the right side, where *di* and d_e represent the distances from a point on the Hirshfeld surface to the nearest atom inside and outside the molecule, respectively, and the sharp spikes correspond to strong close contacts, such as hydrogen bonds, which is consistent with the red regions observed on the d_{norm} surfaces. The analysis shows that the Hirshfeld surfaces of Oxyma-B in all four salts are dominated by HB interactions. Particularly, O···H contacts make the largest contribution, ranging from 31.6% to 34.1%, while H···N interactions contribute the least (1.4-2.2%). H···O (7.4-8.6%) and N···H (4.9-9%) contacts follow. These results verify that the supramolecular assembly in these systems is controlled by strong directional hydrogen bonds. The relative contributions are similar for the four compounds, although compound 3 has a slightly higher N···H contribution (9%), which corresponds to the participation of NH···N and CH···N hydrogen bonds in its supramolecular network.

3.2.1. *DFT calculations*

To complement the structural insights derived from X-ray diffraction analysis, a computational study was undertaken to further elucidate the nature and strength of the hydrogen bonding interactions observed in the crystal structures. Fig. 14 presents partial views of the X-ray crystal structures of salts **1**–**4**, highlighting the most prominent hydrogen-bonding motifs formed between the OXYMA-B anion and the corresponding cations. In compounds **1** and **2**, centrosymmetric tetramers are observed, consisting of two anions bridged by two cations, resulting in a central $R_4^2(8)$ synthon. This motif is flanked on both sides by fused $R_1^2(6)$ motifs, arising bifurcated two acceptors N-H···O, in which each protonated amine forms simultaneous contacts with two acceptor sites of the anion. In compound **3**, a similar 2:2 (cation:anion) assembly is formed, but it adopts a more extended $R_4^3(12)$ synthon, also combined with fused $R_1^2(6)$ rings akin to those seen in compounds **1** and **2**. In contrast, compound **4** displays a distinct supramolecular organization, forming infinite one-dimensional chains rather than the discrete tetramers found in the other salts, and notably lacks the $R_4^n(N)$-type synthons. These rich and diverse hydrogen-bonding patterns underscore the multidentate acceptor ability of the OXYMA-B anion and the strong donor potential of the protonated amines. The DFT study that follows aims to characterize and quantify the key intermolecular synthons observed here, providing insight into their relative energetic contributions through QTAIM analysis.

To initiate the theoretical analysis, the molecular electrostatic potential (MEP) surface of the deprotonated OXYMA-B anion was computed to visualize the spatial distribution of its electron-rich regions and thereby anticipate its hydrogen bond acceptor behavior. MEP surface analysis is a valuable tool for understanding molecular reactivity [34–38]. It helps to identify the most electron-rich and electron-poor regions of a molecule, which in turn allows us to predict the likely sites for nucleophilic and electrophilic attack. including biological As expected for an anionic species, the MEP is negative across the entire molecular surface (Fig. 15). The most negative region (−138 kcal·mol^{-1}) is localized between the oxygen atom of the oxime group (O1) and the adjacent carbonyl oxygen (O2), highlighting a converging area of strong basicity. A similarly negative potential (−132 kcal·mol^{-1}) is found in the vicinity of the oxime nitrogen and the nearest carbonyl oxygen (N1 and O4), reinforcing the prominence of this region as a bidentate acceptor site. Additionally, the N1–O1 bond of the oxime moiety exhibits a notable MEP value of −125 kcal·mol^{-1}. In contrast, the carbonyl oxygens further from the oxime group display moderately less negative potentials, ranging from −94 to −113 kcal·mol^{-1}. This gradient in electrostatic

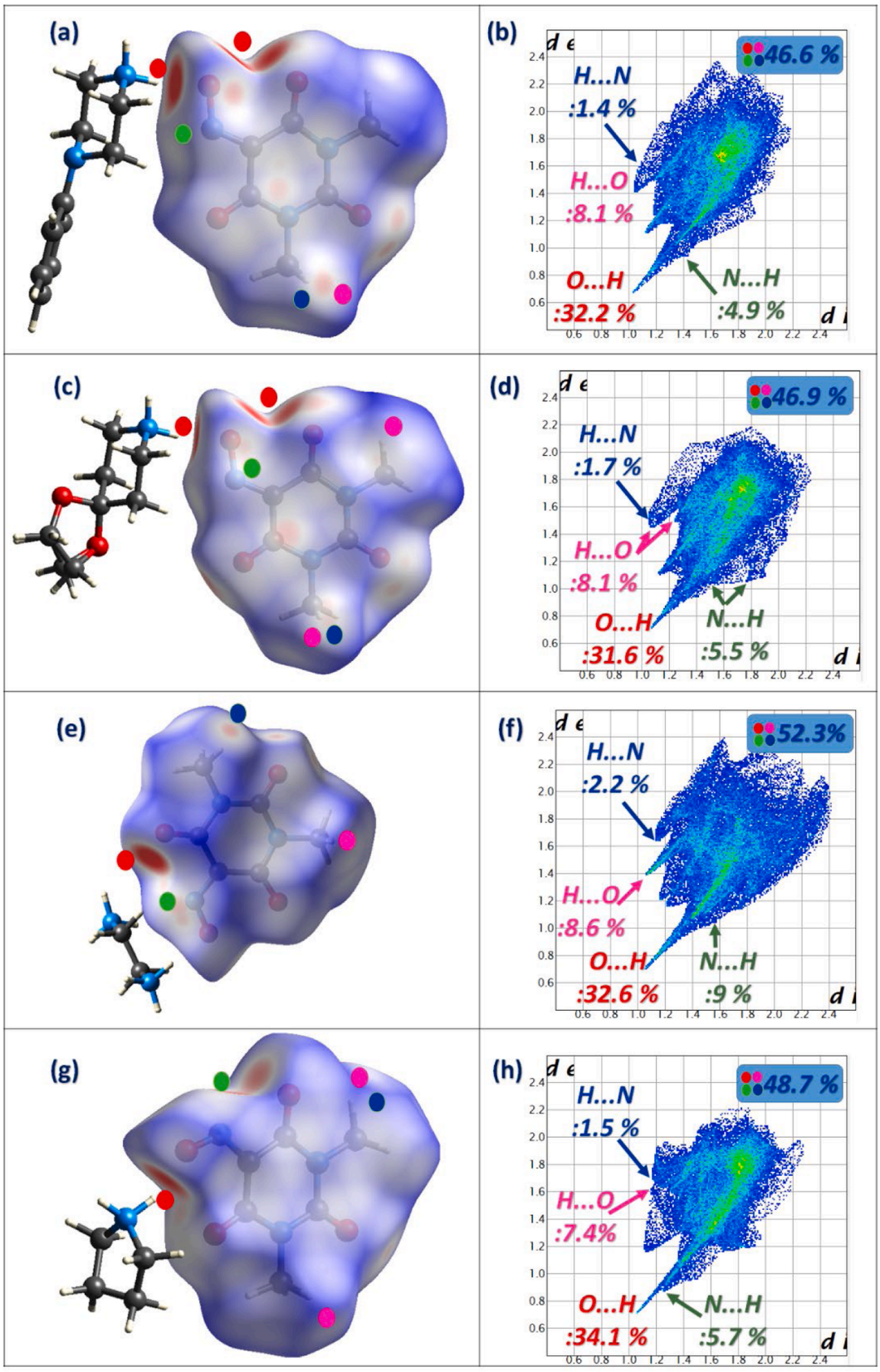

Fig. 13. Hirshfeld surface: d_{norm} mode and fingerprint plots of compounds **1-4**, highlighting the dominant of O···H and N···H contacts.

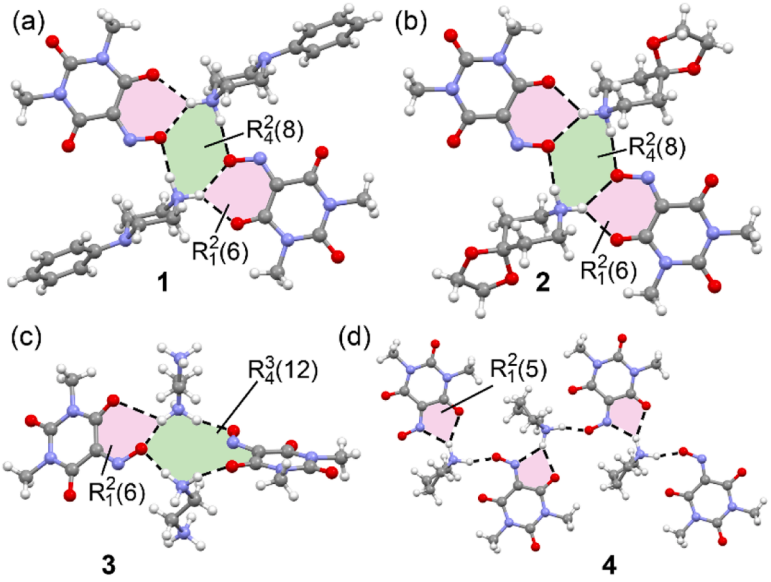

Fig. 14. Partial views of the X-ray structures of **1** (a), **2** (b), **3** (c) and **4** (d) illustrating the different H-bonding synthons. See Table S2-S5 (Supporting Information) for H-bonding distances.

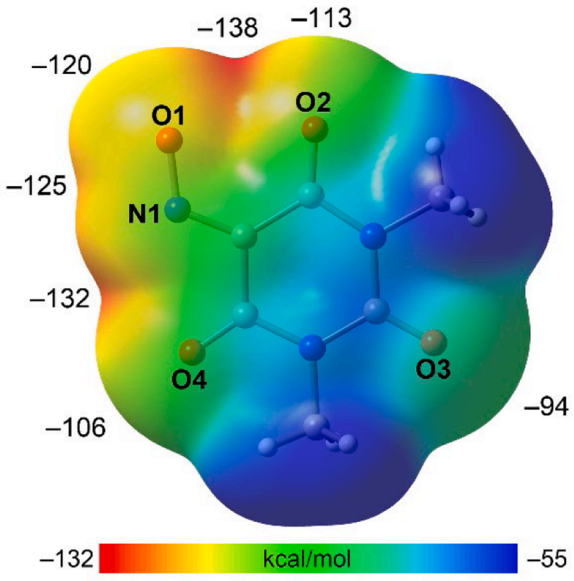

Fig. 15. Molecular electrostatic potential (MEP) surface of the anionic OXYMA-B computed at the PBE0-D4/def2-TZVP level. The MEP is mapped onto the 0.001 a.u. electron density isosurface, with values ranging from −138 to −94 kcal·mol^{-1}.

potential supports the experimentally observed preference for bifurcated N–H···O hydrogen bonds involving the oxime and nearby carbonyl groups.

The QTAIM analysis of compounds **1** and **2**, based on their X-ray geometries, is presented in Fig. 16. Bond critical points (BCPs) are indicated by green spheres, and the corresponding bond paths are shown as dashed lines. The topological analysis confirms the formation of centrosymmetric tetrameric assemblies in both structures, comprising two anions and two cations, and stabilized by multiple hydrogen bonds. Specifically, the canonical $R_4^2(8)$ synthon is clearly identified, flanked by two fused $R_1^2(6)$ motifs involving bifurcated N–H···O,O hydrogen bonds. Each ammonium cation contributes two hydrogen bonds: one forms the bifurcated interaction connecting both carbonyl oxygen atoms of the

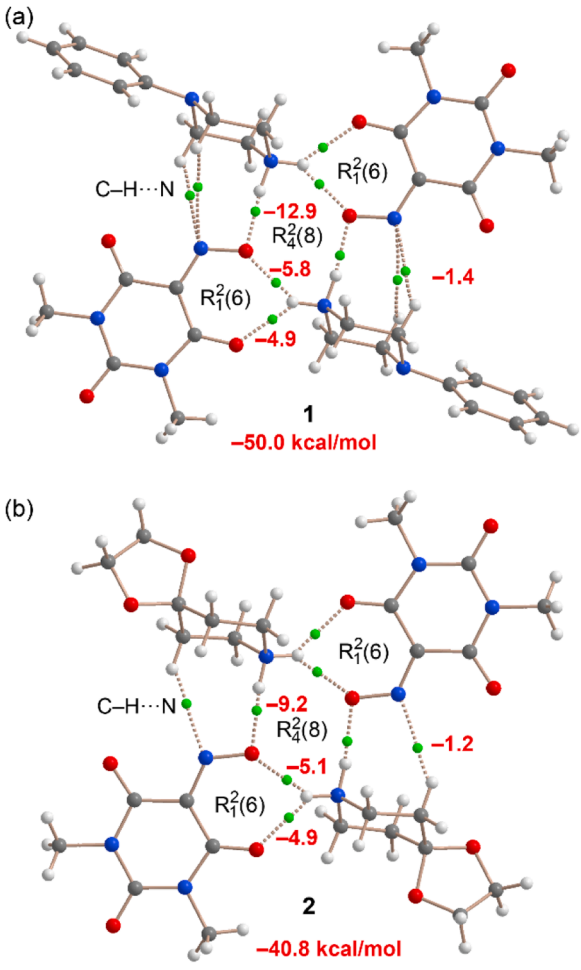

Fig. 16. QTAIM analysis of the hydrogen-bonding networks in the X-ray structures of compounds **1** and **2**. Bond critical points (BCPs) are represented as green spheres, and bond paths are shown as dashed lines. The energy of each H-bond is represented in red adjacent to the BCP in kcal·mol^{-1}.

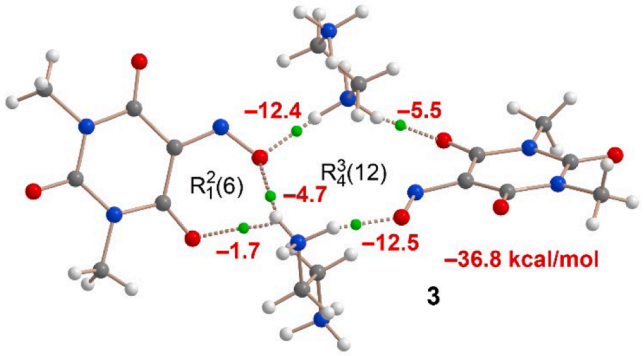

Fig. 17. QTAIM analysis of the hydrogen-bonding network in the X-ray structure of compound 3. Bond critical points (BCPs) are shown as green spheres, and bond paths are indicated by dashed lines. The energy of each H-bond is represented in red adjacent to the BCP in kcal·mol^{-1}.

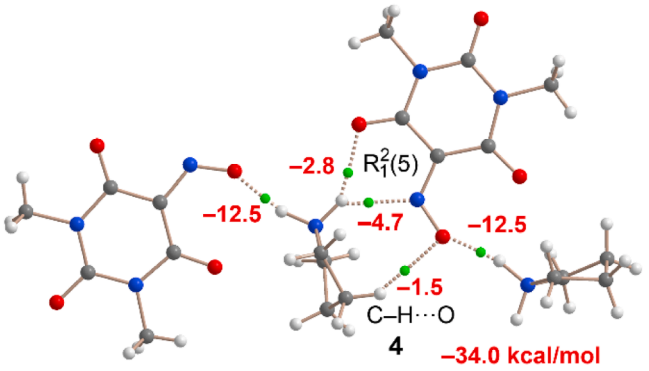

Fig. 18. QTAIM analysis of a tetrameric fragment of the 1D supramolecular chain observed in the crystal structure of compound 4. Bond critical points (BCPs) are depicted as green spheres, and bond paths as dashed lines. The energy of each H-bond is represented in red adjacent to the BCP in kcal·mol^{-1}.

anion, while the second engages in a strong, directional N–H···O contact with the oxime oxygen. The estimated interaction energies, derived from the potential energy density at the BCPs using the empirical relationship proposed by Espinosa et al. [30], indicate that the bifurcated N–H···O,O hydrogen bonds are −10.7 and −10.0 kcal·mol^{-1} compounds **1** and **2**, respectively. The second N–H···O interaction is even stronger, in compound **1** and similar in Compound **2**, with energies of −12.9 and −9.2 kcal·mol^{-1}, respectively. Additionally, weaker C–H···N contacts are identified in both compounds, contributing −1.4 and −1.2 kcal·mol^{-1}, respectively. These cooperative interactions result in total stabilization energies of −50.0 kcal·mol^{-1} (**1**) and −40.8 kcal·mol^{-1} (**2**), underscoring the prominent role of hydrogen bonding in directing the supramolecular organization in the solid state.

The QTAIM analysis of the hydrogen-bonding network in compound **3**(Fig. 17) reveals a supramolecular assembly involving two anions and two cations, analogous to the structures observed in compounds 1 and 2. Specifically, the analysis confirms the presence of a fused $R_1^2(6)$ synthon and a central $R_4^3(12)$ motif. The bifurcated N–H···O,O hydrogen bond within the $R_1^2(6)$ ring is notably weaker (–6.4 kcal/mol) compared to those in compounds **1** and **2**, which can be attributed to suboptimal geometry and longer H···O contact distances, as detailed in Table 1. In contrast, the directional N–H···O hydrogen bonds that define the larger $R_4^3(12)$ synthon are relatively strong (–12.4 and –12.5 kcal/mol), comparable to the energies found in the $R_4^2(8)$ motif of compound **1**. The total stabilization energy of this tetrameric assembly (–36.8 kcal/mol) is lower than those observed in compounds **1** and **2**, primarily due to the weaker bifurcated H-bonding and the lack of auxiliary interactions such as C–H···N contacts.

The QTAIM analysis of compound **4** (Fig. 18) provides a detailed insight into the hydrogen bonding framework that sustains the infinite 1D supramolecular chain observed in its crystal structure. The fragment analyzed includes a tetrameric unit composed of two cations and two anions, which allows a consistent comparison with the assemblies of compounds **1**–**3**. The analysis confirms the formation of an $R_1^2(5)$ synthon through a bifurcated N–H···O,N hydrogen bond (–6.4 kcal/mol), whose energy matches that found for the $R_1^2(6)$ synthon in compound **3** and is weaker than the analogous motifs in compounds **1** and **2**. On the opposite side of the ammonium group, a directional N–H···O hydrogen bond is formed with an energy of –12.5 kcal/mol, comparable to the strongest interactions observed across the series. Additionally, a weak ancillary C–H···O contact (–1.5 kcal/mol) contributes to the stabilization of the assembly. The total interaction energy of this tetrameric unit (–34.0 kcal/mol) is similar to that of compound **3**, confirming that although the R_4^4-type ring is absent in this case, the network remains robust.

In general, this energetic study of the H-bonding interactions supports the notion that the $R_4^2(8)$ central ring combined with adjacent $R_1^2(6)$ units, as found in compounds **1** and **2**, is the most energetically favorable configuration. Nevertheless, packing requirements and complementary interactions such as π-stacking may override this preference in the solid state.

4. Conclusions

In this study, we report the synthesis, structural characterization, and computational analysis of four new salts of OXYMA-B with different amines. X-ray diffraction analysis revealed diverse hydrogen-bonding motifs across the series, with compounds **1**–**3** forming centrosymmetric tetrameric assemblies featuring central $R_4^2(8)$ or $R_4^3(12)$ supramolecular synthons, while compound **4** crystallizes in infinite 1D chains stabilized by $R_1^2(5)$ motifs.

Theoretical analysis based on electrostatic potential (MEP) maps of the OXYMA-B anion confirmed a highly negative potential over the oxime and carbonyl regions, highlighting their strong H-bond acceptor character. QTAIM analysis of the X-ray geometries provided a detailed topological characterization of the H-bonding networks, revealing the presence of bifurcated and directional hydrogen bonds, as well as ancillary C–H···O/N contacts. The individual strengths of these interactions were quantified, showing that directional N–H···O bonds consistently contribute the most to the stability of the assemblies, with ancillary contacts playing a secondary yet supportive role. The total interaction energies, ranging from –34.0 to –50.0 kcal/mol, underscore the critical role of hydrogen bonding in dictating the supramolecular architectures. Notably, the highest stabilization was observed in assemblies featuring the $R_4^2(8)$ synthon flanked by two $R_1^2(6)$ rings, as found in compounds **1** and **2**. These results demonstrate the utility of combining crystallography with DFT-based QTAIM and MEP analyses to rationalize and predict hydrogen bonding patterns in supramolecular salts. This integrated approach provides insights for the future design of functional hydrogen-bonded materials based on OXYMA-B and related systems.

Funding

This research was supported by the Research Project of MICIU/AEI of Spain (projects PID2020-115637GB-I00, PID2023-148453NB-I00 and PID2023-146632OB-I00 FEDER funds).

Availability of data and materials

Crystallographic data have been deposited at the CCDC and can be obtained from https://www.ccdc.cam.ac.uk.

CRediT authorship contribution statement

Mahdi Jemai: Writing – original draft, Investigation, Data curation. **Rafael Barbas:** Investigation. **Miquel Barceló-Oliver:** Investigation. **Houda Marouani:** Investigation. **Fernando Albericio:** Investigation. **Antonio Frontera:** Writing – review & editing, Writing – original draft, Resources, Formal analysis, Conceptualization. **Rafel Prohens:** Writing – review & editing, Writing – original draft, Validation, Supervision, Resources, Conceptualization.

Declaration of competing interest

The authors declare the following financial interests/personal relationships which may be considered as potential competing interests: Rafel Prohens reports financial support was provided by Spain Ministry of Science and Innovation. Antonio Frontera reports financial support was provided by Spain Ministry of Science and Innovation. If there are other authors, they declare that they have no known competing financial interests or personal relationships that could have appeared to influence the work reported in this paper.

Acknowledgments

The authors would like to acknowledge the CTI (UIB) for computational facilities.

Supplementary materials

Supplementary material associated with this article can be found, in the online version, at doi:10.1016/j.molstruc.2025.144488.

References

[1] D. Braga, Crystal engineering, where from? Where to? Chem. Commun. (2003) 2751–2754.
[2] A.K. Nangia, G.R. Desiraju, Crystal engineering: an outlook for the future, Angew. Chem. Int. Ed. 58 (2019) 4100–4107.
[3] B. Bakhshipour, A. Tarahhomi, A. van der Lee, Synthesis and structural study of five new phosphoric triamides: interplay between classical and non-classical intermolecular interactions, Z. Kristallogr. Cryst. Mater. 236 (2021) 301–312.
[4] K.L. Cavanagh, C. Maheshwari, N. Rodríguez-Hornedo, Understanding the differences between cocrystal and salt aqueous solubilities, J. Pharm. Sci. 107 (2018) 113–120.
[5] A. Chettri, A. Subba, G.P Singh, P. Pratim Bag, Pharmaceutical co-crystals: a green way to enhance drug stability and solubility for improved therapeutic efficacy, J. Pharm. Pharmacol. 76 (2024) 1–12.
[6] S. Narala, D. Nyavanandi, P. Srinivasan, P. Mandati, S. Bandari, M.A. Repka, Pharmaceutical Co-crystals, salts, and Co-amorphous systems: a novel opportunity of hot-melt extrusion, J. Drug Deliv. Sci. Technol. 61 (2021) 102209.
[7] P. Sanphuip, A. Nangia, Salts and Co-crystals of theobromine and their phase transformations in water, J. Chem. Sci. 126 (2014) 1249–1264.
[8] C.B. Aakero1, M.E. Fasulo, J. Desper, Cocrystal or salt: does it really matter?, 4 (2007) 317-322.
[9] S.N. Black, E.A. Collier, R.J. Davey, R.J. Roberts, Structure, solubility, screening, and synthesis of molecular salts, J. Pharm. Sci. 96 (2007) 1053–1068.
[10] A.A. Ganie, T.M. Ismail, P.K. Sajith, A.A. Dar, Validation of the supramolecular synthon preference through DFT and physicochemical property investigations of pyridyl salts of organo-sulfonates, New J. Chem. 45 (2021) 4780–4790.
[11] H.R. Rajegowda, B.S. Chethanc, R. Rahaman Khanb, N.K. Lokanathc, P. A. Suchetana, P.R. Kuma, Synthesis, crystal structure and thermal investigation of molecular salts of (R)-1-phenylethanamine combined with quantum chemical studies, J. Mol. Struct. 1272 (2023) 134097.
[12] J. Kołodziejczak, A. Adamczyk-Woźniak, B. Hachuła, M. Barys, H.T. Flakus, A. Sporzyński, A. Koll, Intermolecular interactions in the solid state of ionic secondary Mannich bases, Cryst. Growth Des. 12 (2012) 589–598.
[13] R. Prohens, R. Barbas, M. Barceló-Oliver, A. Frontera, New salt-solvates of Mirabegron: a combined experimental and computational study, 27 (2025) 2720-2728.
[14] S.R. Mannea, B.G. de la Torrea, A. El-Faham, F. Albericio, OxymaPure coupling reagents: beyond solid-phase peptide synthesis, Synthesis 52 (2020) 3189–3210.
[15] R. Barbas, D. de Sande, M. Font-Bardia, R. Prohens, A. Frontera, Revision of the crystal structure of the orthorhombic polymorph of oxyma: on the importance of π–Hole interactions and their interplay with H–Bonds, crystals, 12 (2022) 823.
[16] Y.E. Jad, S.N. Khattab, B.G. de la Torre, T. Govender, H.G. Kruger, A. El-Faham, F. Albericio, Oxyma-B, an excellent racemization suppressor for peptide synthesis, Org. Biomol. Chem. 12 (2014) 8379–8385.
[17] R. Prohens, R. Barbas, B.G. de la Torre, F. Albericio, A. Frontera, An experimental and computational investigation of the elusive anhydrous form of oxyma-B, CrystEngComm 25 (2023) 5818.
[18] Bruker, Bruker AXS Inc (2023).
[19] O.V. Dolomanov, L.J. Bourhis, R.J. Gildea, J.A.K. Howard, H. Puschmann, OLEX2: a complete structure solution, refinement and analysis program, J. Appl. Crystallogr. 42 (2009) 339–341.
[20] G.M. Sheldrick, Crystal structure refinement with SHELXL. Acta crystallogr, C Struct. Chem. 71 (2015) 3–8.
[21] A.L. Spek, Single-crystal structure validation with the program PLATON, J. Appl. Cryst. 36 (2003) 7–11.
[22] M.C. Etter, J.C. MacDonald, J. Bernstein, Graph-set analysis of hydrogen-bond patterns in organic crystals, Acta Crystallogr. B Struct. Sci. Cryst. Eng. Mater. 46 (1990) 256–262.
[23] H. Putz, K. Brandenburg, DIAMOND, Version 3.2k, Crystal Impact GbR, Bonn, Germany, 2014.
[24] Gaussian 16, Revision C.01, M. J. Frisch, G. W. Trucks, H. B. Schlegel, G. E. Scuseria, M. A. Robb, J. R. Cheeseman, G. Scalmani, V. Barone, G. A. Petersson, H. Nakatsuji, X. Li, M. Caricato, A. V. Marenich, J. Bloino, B. G. Janesko, R. Gomperts, B. Mennucci, H. P. Hratchian, J. V. Ortiz, A. F. Izmaylov, J. L. Sonnenberg, D. Williams-Young, F. Ding, F. Lipparini, F. Egidi, J. Goings, B. Peng, A. Petrone, T. Henderson, D. Ranasinghe, V. G. Zakrzewski, J. Gao, N. Rega, G. Zheng, W. Liang, M. Hada, M. Ehara, K. Toyota, R. Fukuda, J. Hasegawa, M. Ishida, T. Nakajima, Y. Honda, O. Kitao, H. Nakai, T. Vreven, K. Throssell, J. A. Montgomery, Jr., J. E. Peralta, F. Ogliaro, M. J. Bearpark, J. J. Heyd, E. N. Brothers, K. N. Kudin, V. N. Staroverov, T. A. Keith, R. Kobayashi, J. Normand, K. Raghavachari, A. P. Rendell, J. C. Burant, S. S. Iyengar, J. Tomasi, M. Cossi, J. M. Millam, M. Klene, C. Adamo, R. Cammi, J. W. Ochterski, R. L. Martin, K. Morokuma, O. Farkas, J. B. Foresman, and D. J. Fox, Gaussian, Inc., Wallingford CT, 2016.
[25] S. Grimme, J. Antony, S. Ehrlich, H. Krieg, A consistent and accurate ab initio parametrization of density functional dispersion correction (DFT-D) for the 94 elements H-Pu, J. Chem. Phys. 132 (2010) 154104.
[26] F. Weigend, R. Ahlrichs, Balanced basis sets of split valence, triple zeta valence and quadruple zeta valence quality for H to Rn: design and assessment of accuracy, Phys. Chem. Chem. Phys. 7 (2005) 3297–3305.
[27] C. Adamo; V. Barone, Toward reliable density functional methods without adjustable parameters: the PBE0 model, 110 (1999) 6158-6170.
[28] R.F.W. Bader, Atoms in Molecules: A Quantum Theory, Oxford University Press, Oxford, 1990.
[29] 6. AIMAll (Version 19.10.12), T. A. Keith, TK Gristmill Software, Overland Park KS, USA, 2019.
[30] E. Espinosa, E. Molins, C. Lecomte, Hydrogen bond strengths revealed by topological analyses of experimentally observed electron densities, Chem. Phys. Lett. 285 (1998) 170–173.
[31] R.R. Choudhury, R. Chitra, Stacking interaction between homostacks of simple aromatics and the factors influencing these interactions, CrystEngComm 12 (2010) 2113–2121.
[32] M.A. Spackman, D. Jayatilaka, Hirshfeld surface analysis, CrystEngComm 11 (2009) 19–32.
[33] M.A. Spackman, J.J. Mckinnon, Fingerprinting intermolecular interactions in molecular crystals, CrystEngComm 4 (2002) 378–392.
[34] S. Kundu, M. Feizi-Dehnayebi, S. Akkoc, Biochem. Biophys. Res. Commun. 780 (2025) 152472.
[35] M. Feizi-Dehnayebi, G.M. Ziarani, T.N. Lohith, S. Ghareghomi, Z. Panahande, M. Farsadrooh, M. Majidinia, J. Mol. Liq. 428 (2025) 127475.
[36] R. Hemmati, A. Abdi, M. Feizi-Dehnayebi, M. Farajzadeh, G.M. Ziarani, A. Banitalebi, A. Badiei, J. Environ. Chem. Eng. 13 (2025) 116981.
[37] S. Jamshidi, A. Eghbalian, S. Shojaei, A. Taherkhani, M. Feizi-Dehnayebi, Cancer Rep. (Hoboken) 8 (2025) e70315.
[38] N. Akın, Y. Sunucu-Karafakıoğlu, S. Akkoc, M. Feizi-Dehnayebi, E. Başaran, I. Ozer Ilhan, Struct. Chem. (2025), https://doi.org/10.1007/s11224-025-02602-7.